Received: 18 March 2020 | Revised: 16 July 2020 | Accepted: 19 July 2020

DOI: 10.1002/jbm.a.37067

ORIGINAL ARTICLE

Development of orthophosphosilicate glass/poly(lactic acid) composite anisotropic scaffolds for simultaneous reconstruction of bone quality and quantity

Sungho Lee[1,2] | Fukue Nagata[1] | Katsuya Kato[1] | Toshihiro Kasuga[3] | Takayoshi Nakano[2]

[1]National Institute of Advanced Industrial Science and Technology (AIST), Nagoya, Japan

[2]Division of Materials and Manufacturing Science, Graduate School of Engineering, Osaka University, Osaka, Japan

[3]Division of Advanced Ceramics, Graduate School of Engineering, Nagoya Institute of Technology, Nagoya, Japan

Correspondence
Sunguo Lee, National Institute of Advanced Industrial Science and Technology (AIST), 2266-78 Anagahora, Shimoshidami, Moriyama-ku, Nagoya 463-8560, Japan (S. L.).
Email: sungho.lee@aist.go.jp

Takayoshi Nakano, Division of Materials and Manufacturing Science, Graduate School of Engineering, Osaka University, 2-1 Yamadaoka, Suita, Osaka 565-0871, Japan (T. N.).
Email: nakano@mat.eng.osaka-u.ac.jp

Funding information
Japan Society for the Promotion of Science, Grant/Award Numbers: 17H06224, 18H05254

Abstract

Reconstruction of organ-specific architecture is necessary to recover the original organ function. The anisotropic structure of bone tissue is strongly related to the collagen fibril alignment and bone apatite crystal direction. Bone regeneration indicates following two main process; first, restoration of bone mineral density (BMD; bone quantity), and second, restoring bone apatite *c*-axis orientation (bone quality). In addition to BMD, bone quality is the most important factor among bone mechanical properties. Recovery of the original bone function requires development of novel scaffolds with simultaneous reconstruction of bone quality and quantity. Herein, novel orthophosphosilicate glass (PSG)/poly(lactic acid) composite anisotropic scaffolds were developed to control cell alignment and enhance bone formation, which are important for the simultaneous reconstruction of bone quality and quantity. The strategy to control cell alignment and bone formation involved designing anisotropic scaffolds in combination with the release of therapeutic ions by PSGs. The morphology of fibrous scaffolds containing PSGs was quantitatively designed using electrospinning. This successfully modulated cell alignment and subsequent bone apatite *c*-axis orientation along the fiber-oriented direction. The released silicate and Mg^{2+} ions from PSGs in scaffolds improved cell adhesion, proliferation, and calcification. To best of our knowledge, this is the first report demonstrating that the anisotropic scaffolds containing bioactive glasses regenerate bone tissues with simultaneous reconstruction of bone quality and quantity via stimulating osteoblasts by inorganic ions and designing morphology of scaffolds.

KEYWORDS

anisotropic scaffold, bioactive glass, bone quality, cell alignment, therapeutic ions

1 | INTRODUCTION

In tissue engineering, restoring the organ-specific architecture is critical to recover their original function. Bone is a highly calcified tissue composed of biological apatite (BAp) crystals and collagen fibrils, which have nano- to microscale hierarchical levels.[1] The multiscale structure of bone tissue indicates anisotropic properties originating from the collagen fibril alignment and direction of the *c*-axis BAp

crystals.[2,3] The degree of BAp *c*-axis orientation, which is one of the major indices for bone quality, correlates well with the Young's modulus of bone tissue.[4] Moreover, the recovery of BAp *c*-axis orientation in the bone regeneration process is significantly retarded compared with restoration of bone mineral density (BMD, bone quantity), which can lead to severe mechanical dysfunction. Hence, bone quality, represented by the anisotropic microstructure of bone tissue, is a predominant mechanical property of bone tissue, rather than bone quantity.[4,5] The development of scaffolds for the simultaneous reconstruction of bone quality and quantity is important for the recovery of their original functions.

Control of osteoblast alignment is one of the strategies for reconstructing bone quality, that is, the anisotropic microstructure of bone tissue.[6] The apatite/collagen matrix alignment in calcified tissues can be determined by osteoblast orientation. The degree of BAp *c*-axis orientation for calcified tissues depends on the directional distribution of osteoblasts.[6–8] Electrospinning is a useful method for producing fibrous scaffolds. These scaffolds are applicable in a biomimetic template for damaged tissue.[9,10] Human mesenchymal stem cells on the oriented nanofiber scaffolds can be aligned to the long axis of the fibers, and produce collagen fibril bundles that are also aligned in the same direction.[11,12] Hence, control of osteoblast alignment by anisotropic morphology could be effective for reconstruction of bone quality.

Bioactive glasses, such as Bioglass 45S5[13,14] and other compositions based on silicate or phosphate systems, have been enhanced with bioactivity related to osteogenesis and angiogenesis by the release of therapeutic ions.[15] Therapeutic inorganic ions, such as silicate, phosphate, Mg^{2+}, Zn^{2+}, and Ca^{2+} ions, have been reported to enhance bone formation. Silicate and Ca^{2+} ions stimulate the proliferation of osteoblasts by increasing the production of insulin-like growth factor II (IGF-II)[16] and upregulate parameters of osteoblast differentiation, such as alkaline phosphatase (ALP) and osteocalcin (OCN).[17] Phosphate ions are the main components of bone. These ions stimulate the expression of the matrix Gla protein, which is a key regulator of bone formation.[18] Mg^{2+} ions enhance cell adhesion, proliferation, differentiation, and mineralization.[19] Zn^{2+} ions upregulate ALP, osteopontin (OPN), and OCN,[20–22] and enhance bone formation by increasing Runx2-targeted osteoblast differentiation gene transcription.[23] Ca^{2+} ions increase the expression of IGF-I and -II,[24] and enhance osteoblast differentiation and calcification of the extracellular matrix.[25]

Phosphate invert glasses (PIG) were developed by our group for biomedical applications.[26–29] PIGs easily introduce therapeutic ions and control their release.[30–32] The use of PIGs stimulates bioactivity in vitro and in vivo.[33–35] Recently, orthophosphate (OPG) and orthophosphosilicate (PSG) glasses were developed using the melt-quenching method. Unique glass network structures free of long chain structures were described.[36–38] PSG contains P–O–Ca and Si–O–Mg bonds, which easily hydrolyze in an aqueous solutions.[37] PSG exhibits excellent ion-releasing ability compared with PIGs.[32] PSG can be a carrier of therapeutic ions for composite biomaterials and is expected to enhance bone formation (i.e., bone quantity).

The aim of this work is to develop a scaffold for the simultaneous reconstruction of bone quality and quantity. Cell alignment can be controlled with an anisotropic fibrous scaffold.[11,12] We previously demonstrated the success of anisotropic scaffolds in controlling osteoblast alignment by virtue of the scaffold morphology,[39,40] and also manipulated the degree of BAp *c*-axis orientation.[41] Other authors described the adherence of cells to a single fiber when the fiber diameter was greater than 10 μm, whereas cells adhered to several fibers and spread when the diameter was less than 10 μm.[42] Thus, cell alignment is readily controlled by the morphology of the scaffolds, specifically cell adherence to a single fiber. The anisotropic scaffolds used in this work were designed to have a fiber diameter greater than 10 μm to control cell alignment. Poly(lactic acid) (PLLA) was chosen to prepare the anisotropic scaffolds to control cell alignment that was strongly related to the construction of anisotropic extracellular matrix (bone quality). PLLA is the most widely used biodegradable polymer in the biomaterial field. PSG containing CaO and ZnO were used as the carriers of therapeutic ions for the anisotropic scaffolds, such as silicate, phosphate, Mg^{2+}, Ca^{2+}, and Zn^{2+} ions, which are expected to enhance bone formation (bone quantity). We report the development of anisotropic scaffolds for the simultaneous reconstruction of bone quality and quantity.

2 | MATERIALS AND METHODS

2.1 | Preparation and characterization of orthophosphosilicate glasses

2.1.1 | Preparation of orthophosphosilicate glasses

Orthophosphosilicate glasses comprised of $15CaO{\cdot}15MgO{\cdot}8P_2O_5{\cdot}4SiO_2$ (molar ratio, PSG-Ca) and $15ZnO{\cdot}15MgO{\cdot}8P_2O_5{\cdot}4SiO_2$ (molar ratio, PSG-Zn) were prepared by a melt-quenching method. The glass batches were manually mixed with MgO (99.0%), $CaCO_3$ (99.5%), ZnO (99.5%), H_3PO_4 (85.0%, liquid), and SiO_2 (99.0%), and were oven dried at 140°C. All reagents were purchased from Kishida Chemical Co. The resulting products were melted in a platinum crucible at 1,500°C for 30 min. The melts were quenched by pressing two stainless plates. The compositions of the glasses were determined by inductively coupled plasma atomic emission spectroscopy (ICP-AES) using an ICPS-8100 apparatus (Shimadzu) and an aqueous solution prepared by dissolving 2.5 mg of the glass powder in 10 ml of 1 N HNO_3. The obtained glass density was measured by an Archimedes method with glass pieces of 200–500 mg using acetone as the immersion fluid (n = 5).

2.1.2 | Structural analysis of the orthophosphosilicate glasses

The glass structures were evaluated using laser Raman spectroscopy (NRS-5100; 532.02 nm, 5.7 mW, 220–1,300 cm^{-1}; JASCO) and solid-

state magic angle-spinning nuclear magnetic resonance (MAS-NMR) spectroscopy. ^{31}P MAS-NMR spectra were evaluated with a pulse width of 3.0 μs, recycle delay of 60 s, and cumulative number of 256 (3.2 mm rotor spinning at 15 kHz, resonance frequency 242.85 MHz; VNS600, Agilent Technologies). Ammonium dihydrogen phosphate ($NH_4H_2PO_4$, 1.0 ppm) was used as a reference to analyze the chemical shifts. ^{29}Si MAS-NMR spectra were evaluated with a pulse width of 7.5 μs, recycle delay of 240 s, and a cumulative number of 700 (8.0 mm rotor spinning at 5 kHz, resonance frequency 119.24 MHz; JNM-ECA600II, JEOL). 3-(Trimethylsilyl)-1-propanesulfonic acid sodium salt (0.0 ppm) was used as a reference to analyze the chemical shifts.

2.1.3 | Ion-release behavior of orthophosphosilicate glasses

Glass powders for ion-release tests were prepared by grinding and sieving (125–250 μm). Fifteen milligrams of glass powders were immersed in 15 ml of 50 mM tris(hydroxymethyl)aminomethane (Tris) buffer solution (TBS, pH 7.40, 37°C) for 7 days. The release of Mg^{2+}, Ca^{2+}, Zn^{2+}, phosphate, and silicate ions into the TBS were measured by ICP-AES. The molar-release fractions for the ions were calculated using the following equation[36–38]:

$$\text{Release percentage}\,(\%) = \frac{(a/M_{\text{wa}}) \times 10^5}{(\text{Frac}_{\text{m,a}} \times M_{\text{w,glass}})/(m_{\text{glass}} \times V_{\text{solution}})} \quad (1)$$

where, a is the concentration of the element of interest in mg/L, M_{wa} is the atomic weight of the respective element, $\text{Frac}_{\text{m,a}}$ is the nominal molar fraction of the element in the glass, $M_{\text{w,glass}}$ is the molecular weight of the glass, m_{glass} is the mass of the sample soaked, and V_{solution} is the volume of TBS. The glass powders before and after soaking in TBS were evaluated by X-ray diffractometry (XRD; Cu Kα, 1.54 Å; X'pert PRO, Phillips).

2.2 | Preparation and characterization of anisotropic scaffolds

2.2.1 | Preparation of orthophosphosilicate glass/poly(lactic acid) composite anisotropic scaffolds

PSG-Ca and PSG-Zn were pulverized using an automatic alumina mortar, and subsequently ball-milled for 12 hr with methanol (99.8%, Kishida Chemical Co.) as a solvent. The slurries were dried at 70°C for 3 hr and the resulting powders were completely dried overnight at 200°C. The powders were observed by field emission scanning electron microscopy (SEM) operating at 15 kV using a model JSM-6500 microscope (JEOL) after coating with an amorphous osmium layer (Neoc CS; Meiwafosis Co. Ltd.). The diameter of the powders was measured using ImageJ software (NIH) by Feret diameter estimation.

The anisotropic scaffolds were fabricated by an electrospinning method. PLLA pellets (LACEA, Mitsui Chemical) were dissolved in chloroform (99.0%, Wako Pure Chemical) at 14 wt%. Subsequently, PSG-Ca and PSG-Zn powders were added to the PLLA/chloroform solution and dispersed into the solution using a magnetic stirrer (VPS-150S3, AsOne) for electrospinning. The volume ratio of PSG-Ca and PSG-Zn powders in the scaffolds was designed 10 and 30 vol%. The volumes of PSG-Ca, PSG-Zn, and PLLA were calculated from their density. In addition, PLLA solution without glass powder was prepared as a control for the cell culture test. The prepared solutions were loaded into a syringe equipped with an 18-gauge needle and extruded at a discharge rate of 2.5 μl/s (FP-1100, Melquest). The distance between the drum collector and needle tip was set to 200 mm, with an applied voltage of 25 kV (HARb-40P0.75, Matsusada Precision Inc.) at the needle tip. The collection speed of the drum collector (φ 30 mm) was 4.7 m/s (3,000 rpm). The obtained scaffolds were denoted PSG-*x*Ca and PSG-*x*Zn, where *x* is the vol% of PSG-Ca and PSG-Zn in the scaffolds. Electrospinning was performed at room temperature (~25°C) and approximately 40% relative humidity.

2.2.2 | Morphology of anisotropic scaffolds

The morphology of the anisotropic scaffolds was observed using SEM at an operating voltage of 3 kV after coating with an amorphous osmium layer. The fiber diameter and angle (θ) between the fiber and collector rotation direction were estimated using ImageJ software. PSG-*x*Ca and PSG-*x*Zn were molded in epoxy resin, sliced into approximately 2 mm pieces, and mirror-polished. Cross-sectioned samples were observed by SEM (15 kV; S-4300, Hitachi) after coating with an amorphous osmium layer (Neoc-Pro, Meiwafosis Co. Ltd.). Ca element mapping images of PSG-*x*Ca were obtained by energy dispersive X-ray spectroscopy (EDX) using an EX-200 apparatus (Horiba).

2.2.3 | Ion-release behavior of anisotropic scaffolds

The scaffolds for the ion-release test were prepared with 14 mm diameter, thickness of 120–160 μm, and weight of 7–12 mg. The scaffolds were immersed in 10 ml of TBS (pH 7.40, 37°C) for 12 days. Concentrations of Mg^{2+}, Ca^{2+}, Zn^{2+}, phosphate, and silicate ions in TBS were evaluated using ICP-AES. The fraction of weight released of various elements in TBS is calculated as follows[39];

$$\text{Release precentage}\,(\%) = \frac{b \times V_{\text{solution}}}{m_{\text{scaffold}} \times W_{\text{glass}} \times \text{Frac}_{\text{w,b}}} \quad (2)$$

where, b is the concentration of the element of interest in mg/L, $V_{solution}$ is the volume of the soaked solution in L, $Frac_{w,b}$ is the nominal weight fraction of the element in the glass, $m_{scaffold}$ is the weight of the sample, and W_{glass} is wt% of the glass in the scaffold. After soaking in TBS for 12 days, the scaffolds were analyzed by XRD.

2.3 | Cell behaviors on anisotropic scaffolds

2.3.1 | Osteoblast proliferation

Osteoblast proliferation test was performed on scaffolds with 8 mm diameter, and a PLLA anisotropic scaffold was used as a control. The scaffolds were sterilized by soaking in 70% ethanol for 30 s and drying under ultraviolet light for 30 min. The scaffolds were then placed into 48 well plates (n = 3). The culture medium prepared with alpha-minimum essential medium (α-MEM, Invitrogen) containing 10% fetal bovine serum (Invitrogen). Mouse osteoblast-like cells (MC3T3-E1 cells) were seeded into the scaffolds by adding 0.5 ml with cell concentration of 3×10^4 cells/mL. The culture medium was replaced after days 1 and 3, and every 3 days thereafter. After the culture preset period, the scaffolds were washed with phosphate buffered saline (PBS) and added to 0.5 ml of α-MEM (without phenol red, Invitrogen). Subsequently, 50 μl of Cell Count Reagent SF (Nacalai Tesque) was added to each well, and absorbance was measured at 450 nm using a Multiskan FC instrument (Thermo Fisher Scientific) after 2 hr of incubation (37°C, 5% CO_2). The number of cells was estimated using the standard curve between the number of cells and absorbance of the resulting medium.

2.3.2 | Primary osteoblast isolation

Primary osteoblasts were isolated from newborn mouse calvaria as we described previously.[43,44] Calvariae were excised from newborn C57BL/6 mice, and fibrous tissues were gently removed in ice-cold α-MEM. A series of digestions using collagenase (Wako Pure Chemical)/trypsin (Nacalai Tesque) were performed at 37°C for 15 min for calvaria. The first two digests were discarded since fibroblasts were mixed.[45] The supernatants of digests three to five were neutralized with α-MEM, pooled, and filtered using a 100 μm mesh. The filtrate was centrifuged, and the resulting pellet was suspended in α-MEM. All animal experiments were approved by the Osaka University Committee for Animal Experimentation.

2.3.3 | Cultivation of primary osteoblasts on anisotropic scaffolds

The scaffolds (φ 8 mm) were sterilized by soaking in 70% ethanol for 30 s and drying under ultraviolet light for 30 min. The scaffolds were placed into 48 well plates. Primary osteoblasts were seeded on the scaffolds by adding 0.5 ml with a cell concentration of 3×10^4 cells/ml. The culture medium was replaced after day 1 and 3, and subsequently two times per week. After culturing for a week, the medium was adjusted to a final concentration of 50 μg/ml ascorbic acid (Sigma-Aldrich), 10 mM β-glycerophosphate (Sigma-Aldrich), and 50 nM dexamethasone (MP Bioscience).[6,46] The samples used to analyze cell orientation and to evaluate calcified tissues were cultured for 3 days and 6 weeks, respectively.

2.3.4 | Fluorescence imaging of primary osteoblasts

The scaffolds (n = 3) cultured for 3 days with primary osteoblasts were fixed with 4% formaldehyde in PBS for 20 min and washed three times with PBS-0.05% Triton X-100 (PBST). To block nonspecific antibody-binding sites, the cells on the scaffolds were treated with 1% normal goat serum (Invitrogen) in PBST for 30 min. The cells on scaffolds incubated with primary antibody to mouse monoclonal antibodies against vinculin (Sigma-Aldrich) at 4°C for 12 hr and washed three times with PBST. The cells on the scaffolds were incubated with Alexa Fluor 546-conjugated anti-mouse IgG (Invitrogen) and Alexa Fluor 488-conjugated phalloidin (Invitrogen), and washed three times with PBST. Subsequently, the cells on the scaffolds were mounted in Fluoro-KEEPER antifade reagent containing 4′,6-diamidino-2-phenylindole (DAPI; Nacalai Tesque). The cell orientation angle (θ) against the collector rotation direction was assessed using Cell Profiler software (Broad Institute Cambridge) from fluorescent images obtained using a model BZ-X700 microscope (Keyence).

2.3.5 | Alizarin red S staining of calcified tissues

To visualize and analyze calcified tissues (culturing for 6 weeks), samples were fixed with 4% formaldehyde in PBS for 20 min and washed with distilled water. The samples (n = 3) were stained with 0.25 ml of 1% Alizarin red S staining solution (pH 4.2, Wako Pure Chemical) for 30 min. Excess stain was washed off with distilled water. Images were obtained with a model BZ-X700 microscope (Keyence). The stained area ratio was determined using ImageJ software (φ 6 mm at center). To quantitatively evaluate calcified tissues by primary osteoblasts, the samples were soaked in 0.25 ml of 5% formic acid for 10 min. The solutions (100 μl) were measured using a microplate reader at an absorbance of 450 nm.[47]

2.3.6 | Microbeam X-ray diffraction analysis of calcified tissues

Apatite crystals produced by primary osteoblasts were evaluated using a microbeam X-ray diffraction system (R-Axis BQ, Rigaku) with a transmission optical system (Mo-Kα radiation, 0.71 Å, 50 kV, and 90 mA) and an imaging plate (storage phosphors, Fuji Film) placed behind the samples. Detailed conditions for measurement have been previously described.[41,48,49] Presently, the incident beam was focused at φ 800 μm, and diffraction data were collected for 1,200 s. The samples (n = 5) for

evaluation of the calcified tissues (cultured for 6 weeks) were fixed with 4% formaldehyde in PBS for 20 min. The preferred orientation of the apatite *c*-axis was assessed as the relative intensity ratio of the 002 diffraction peak to the 310 peak, which was measured in parallel to the collector rotation direction of the scaffolds. The intensities of the 002 and 310 peaks obtained from the reconstructed patterns were obtained using a multipeak fitting package (Igor Pro, WaveMetrics).

2.4 | Quantitative analysis of the degree of fiber and cell orientation

The orientation order parameters *FD* and *CD* were assessed to evaluate the degrees of fiber and cell alignment. The values of *FD* and *CD* are determined by the following equations[50]:

$$< \cos^2\theta > = \frac{\int_0^{2\pi} \cos^2\theta \cdot n(\theta)\, d\theta}{\int_0^{2\pi} n(\theta)\, d\theta} \quad (3)$$

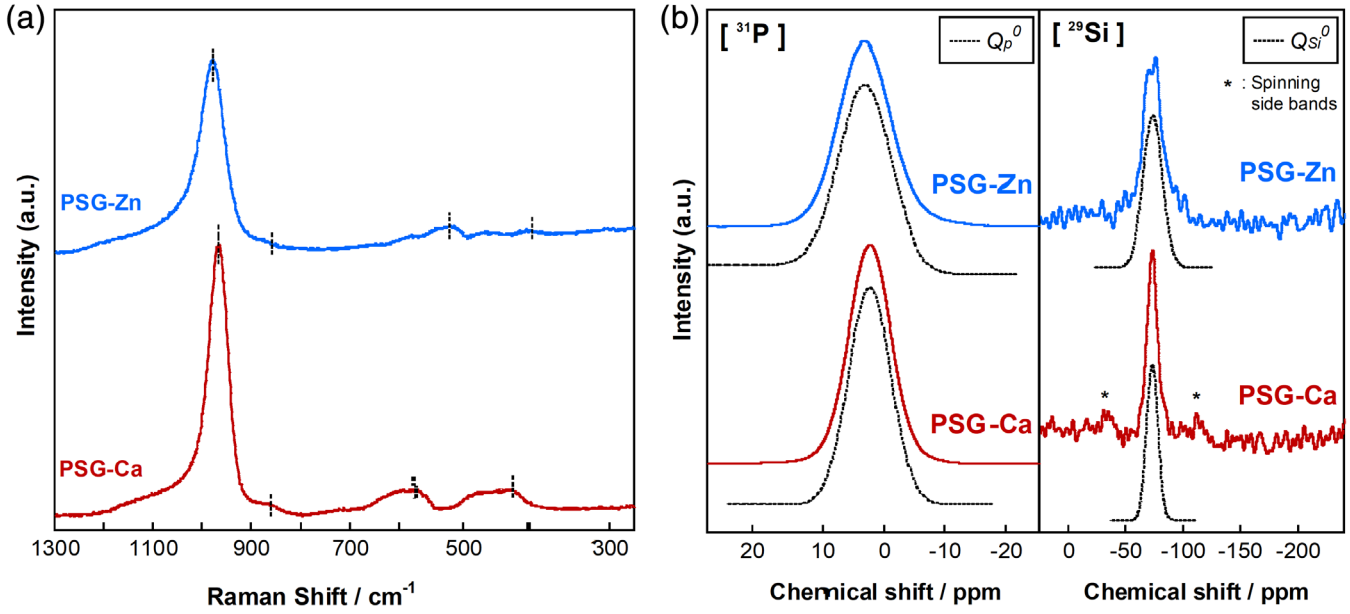

FIGURE 1 (a) Laser Raman spectra of PSG-Ca and PSG-Zn. (b) ^{31}P (left) and ^{29}Si (right) MAS-NMR spectra of PSG-Ca and PSG-Zn. Dotted lines represent the Gaussian curves fitted to the spectra

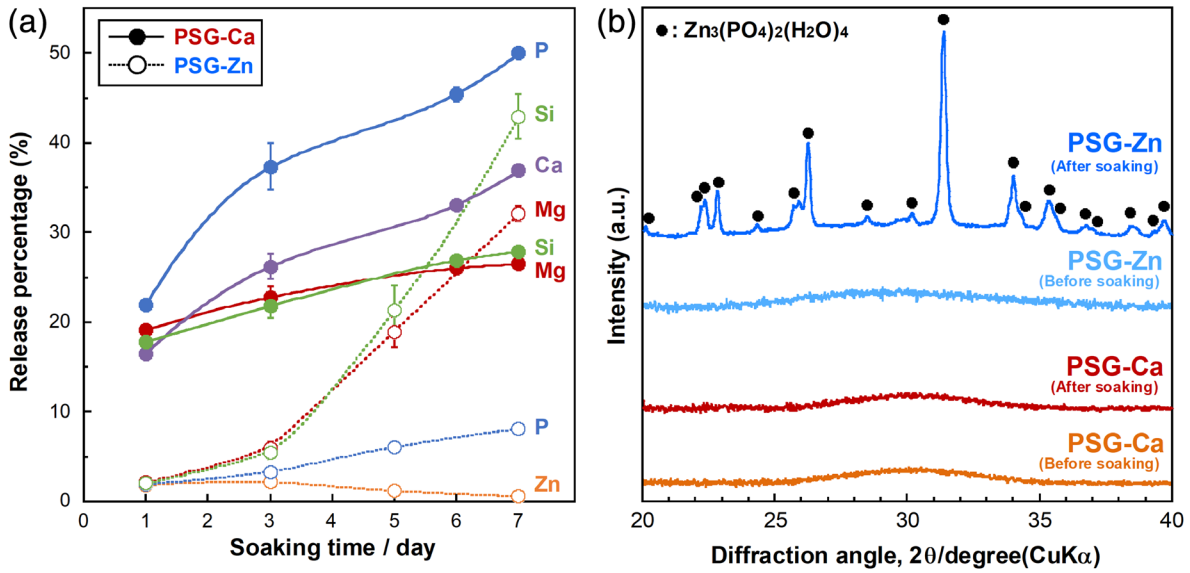

FIGURE 2 (a) Percentage of ions released into TBS from PSG-Ca (solid line) and PSG-Zn (dotted line). (b) XRD patterns of PSG-Ca and PSG-Zn before and after soaking in TBS for 7 days

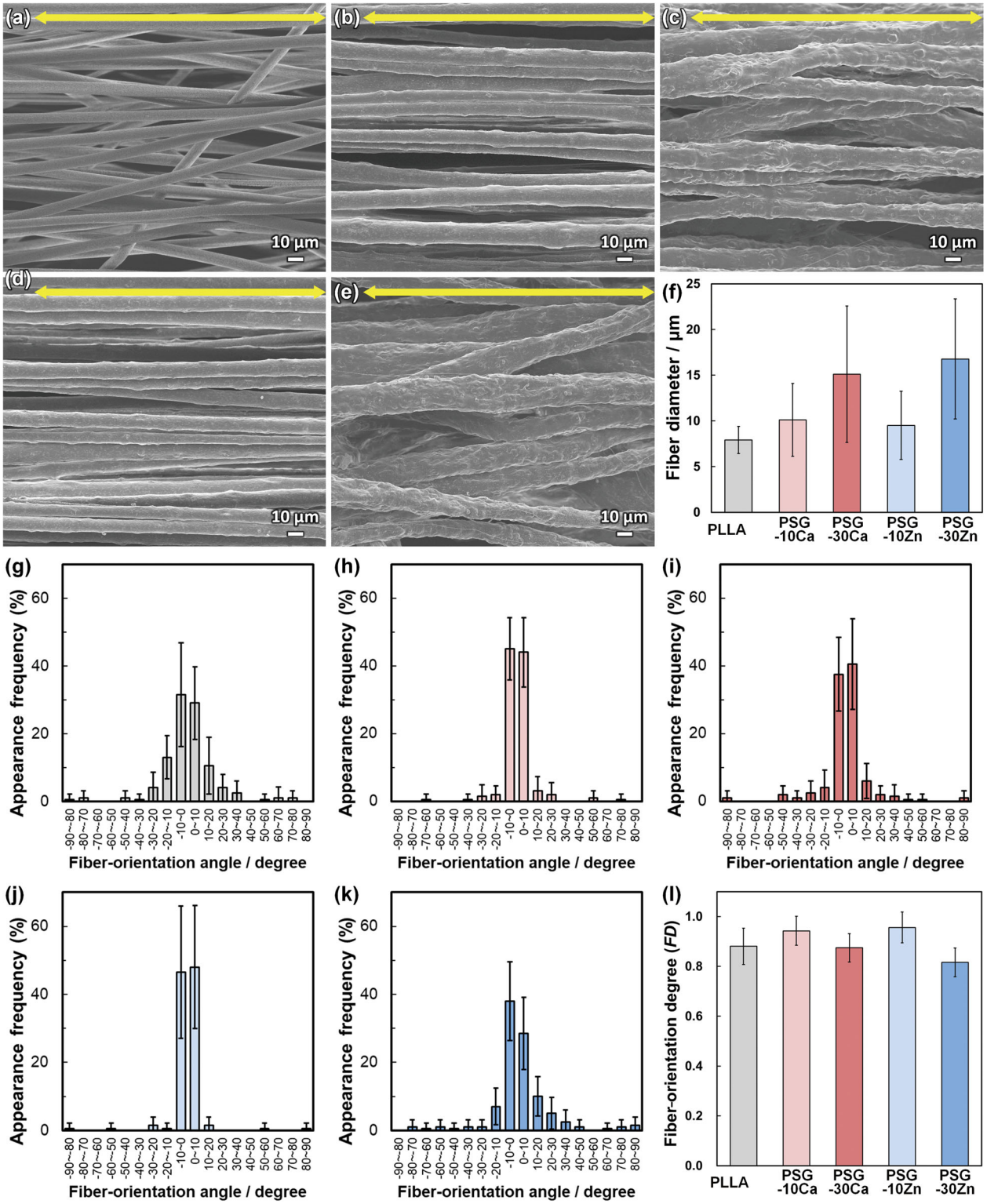

FIGURE 3 SEM images of (a) PLLA, (b) PSG-10Ca, (c) PSG-30Ca, (d) PSG-10Zn, and (e) PSG-30Zn. The yellow arrows indicate the collector rotation direction (0°). (f) Fiber diameter of the anisotropic scaffolds. Fiber orientation-angle histograms for (g) PLLA, (h) PSG-10Ca, (i) PSG-30Ca, (j) PSG-10Zn, and (k) PSG-30Zn. (l) Fiber orientation degree of the anisotropic scaffolds. Error bars represent the standard deviation

$$FD \text{ or } CD = 2\left(< \cos^2\theta > -0.5 \right) \quad (4)$$

FD or *CD* indicates a value ranging from −1 (fiber or cell completely oriented perpendicular to the collector rotation direction), 0 (fiber or cell aligned randomly), to 1 (fiber or cell completely oriented parallel to the collector rotation direction).

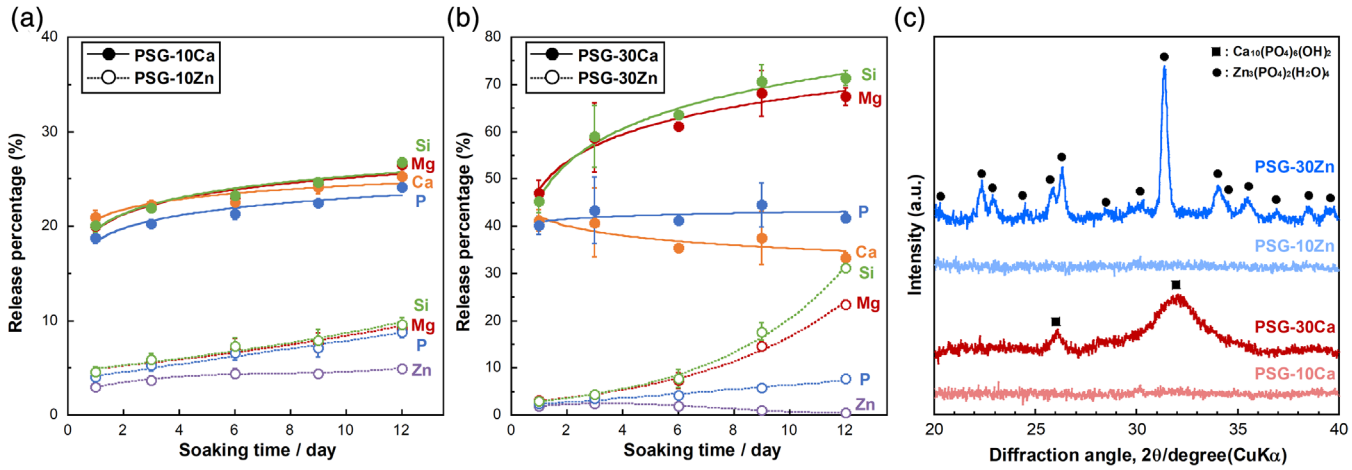

FIGURE 4 Percentage of ions released into TBS from (a) PSG-10Ca and PSG-10Zn, and (b) PSG-30Ca and PSG-30Zn. Error bars represent the standard deviation. (c) XRD patterns of PSG-*x*Ca and PSG-*x*Zn after soaking in TBS for 12 days

2.5 | Statistical analysis

Statistical comparisons between the two means were performed using a two-tailed unpaired Student's *t* test followed by an *F*-test for homoscedasticity. The $p < 0.05$ was considered significant.

3 | RESULTS

3.1 | Characterization of orthophosphosilicate glasses

The obtained PSG-Ca and PSG-Zn were optically clear. The XRD patterns of the glasses showed halo peaks (Figure 2b, before soaking), indicating that the glasses were amorphous in nature. The compositions were $(14.73 \pm 0.01)CaO{\cdot}(15.97 \pm 0.02)MgO{\cdot}(7.60 \pm 0.02)P_2O_5{\cdot}(3.70 \pm 0.01)SiO_2$ and $(14.53 \pm 0.05)ZnO{\cdot}(15.55 \pm 0.02)MgO{\cdot}(7.88 \pm 0.04)P_2O_5{\cdot}(4.04 \pm 0.02)SiO_2$ (mol ratio). These agreed well with the nominal compositions. The densities of PSG-Ca and PSG-Zn were 2.98 ± 0.01 and 3.50 ± 0.03 g/cm^3, respectively. Laser Raman spectra of PSG-Ca and PSG-Zn are shown in Figure 1a. Raman bands corresponding to orthophosphate (Q_p^0) and orthosilicate (Q_{Si}^0) groups were observed.[51–53] Bands corresponding to the $(PO_4)_{sym}$ stretching mode of the nonbridging oxygen in Q_p^0 (~980 cm^{-1}), the symmetric stretching mode of Q_{Si}^0 (~865 cm^{-1}), the symmetric stretching mode of the P–O bond in Q_p^0 (~580 cm^{-1}), and the O–P–O bending mode of Q_p^0 (~430 cm^{-1}) were observed. The ^{31}P and ^{29}Si MAS-NMR spectra of PSG-Ca and PSG-Zn are presented in Figure 1b. The spectra were fit to Gaussian functions (plotted with dotted lines). The ^{31}P MAS-NMR spectra exhibited a peak between −15 and 15 ppm centered at 2.3 and 2.2 ppm for PSG-Ca and PSG-Zn, respectively, which is assigned to Q_p^0.[53] The ^{29}Si MAS-NMR spectra showed a peak between −120 and −40 ppm centered at −73.1 and −73.5 ppm for PSG-Ca and PSG-Zn, respectively, which are assigned to Q_{Si}^0.[54]

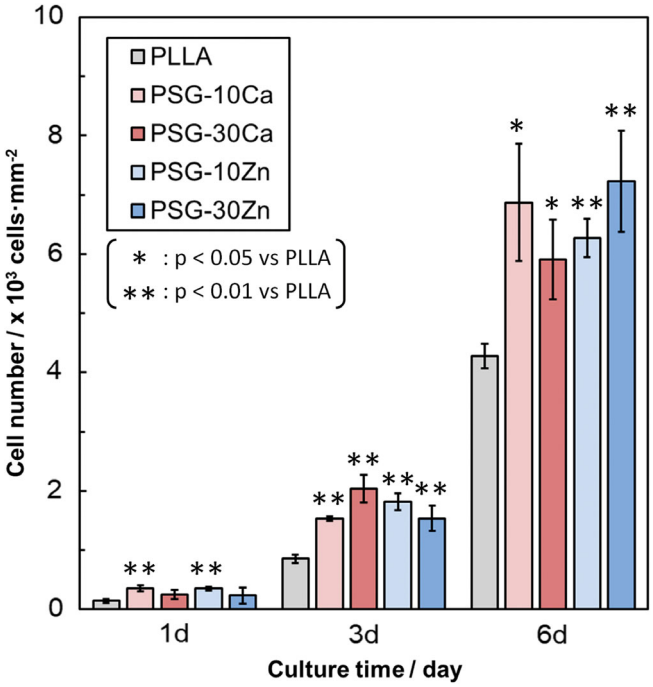

FIGURE 5 MC3T3-E1 cell numbers after 1 to 6 days on PSG-*x*Ca and PSG-*x*Zn. Error bars represent the standard deviation

The ion-release percentages from PSG-Ca and PSG-Zn into TBS, relative to the original amount in the glasses, are shown in Figure 2a. The amount of silicate, phosphate, and Mg^{2+} ions released from PSG-Ca and PSG-Zn increased with increasing soaking time. The amount of phosphate ion released from PSG-Zn was less than that of PSG-Ca. Ca^{2+} ions released from PSG-Ca increased with increasing soaking time, whereas dissolution of Zn^{2+} ions from PSG-Zn decreased to 0% at day 7. The XRD patterns of PSG-Ca and PSG-Zn are shown in Figure 2b. The patterns of the glasses before soaking showed halo peaks, which indicated an amorphous nature. A halo peak was also evident after soaking of PSG-Ca. PSG-Zn exhibited peaks corresponding to hopeite $(Zn_3(PO_4)_2(H_2O)_4$, ICDD card: 76-0896).

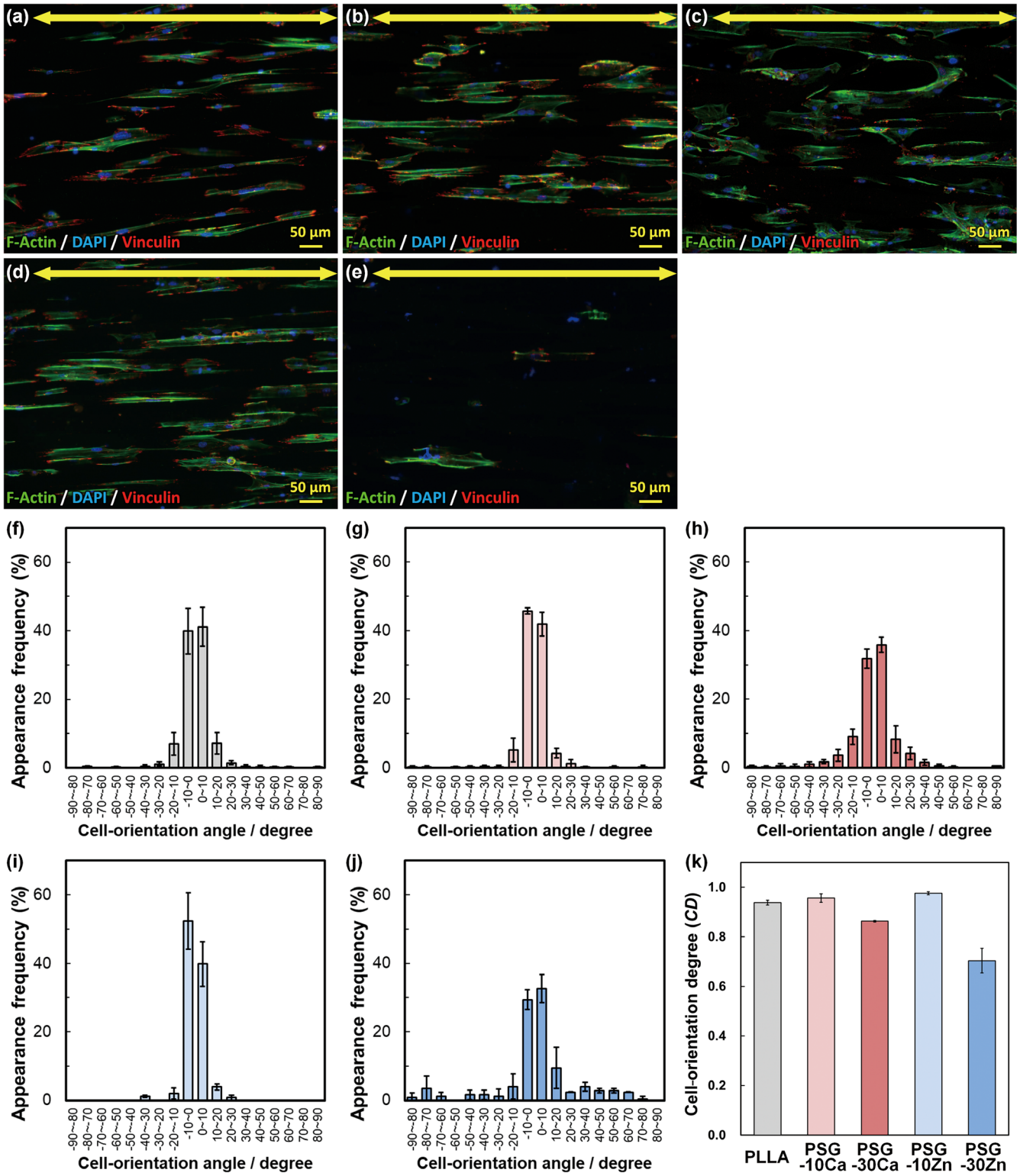

FIGURE 6 Fluorescence images of primary osteoblasts after 3 days of culture on (a) PLLA, (b) PSG-10Ca, (c) PSG-30Ca, (d) PSG-10Zn, and (e) PSG-30Zn. The yellow arrows indicate the collector rotation direction (0°). Green: F-Actin, blue: Nuclei, and red: Vinculin. Cell orientation angle histograms for (f) PLLA, (g) PSG-10Ca, (h) PSG-30Ca, (i) PSG-10Zn, and (j) PSG-30Zn. (k) Cell orientation degree of the anisotropic scaffolds. Error bars represent the standard deviation

3.2 | Characterization of anisotropic scaffolds

The diameter of the PSG-Ca and PSG-Zn ball-milled powders was 5.32 ± 2.43 and 4.91 ± 2.20 μm, respectively. The powder diameters showed no significant difference between PSG-Ca and PSG-Zn. SEM images and fiber orientation histograms of the scaffolds are shown in Figure 3a–e,g–k, respectively. The fibers were oriented with the collector rotation direction (parallel to the yellow arrows). The fiber

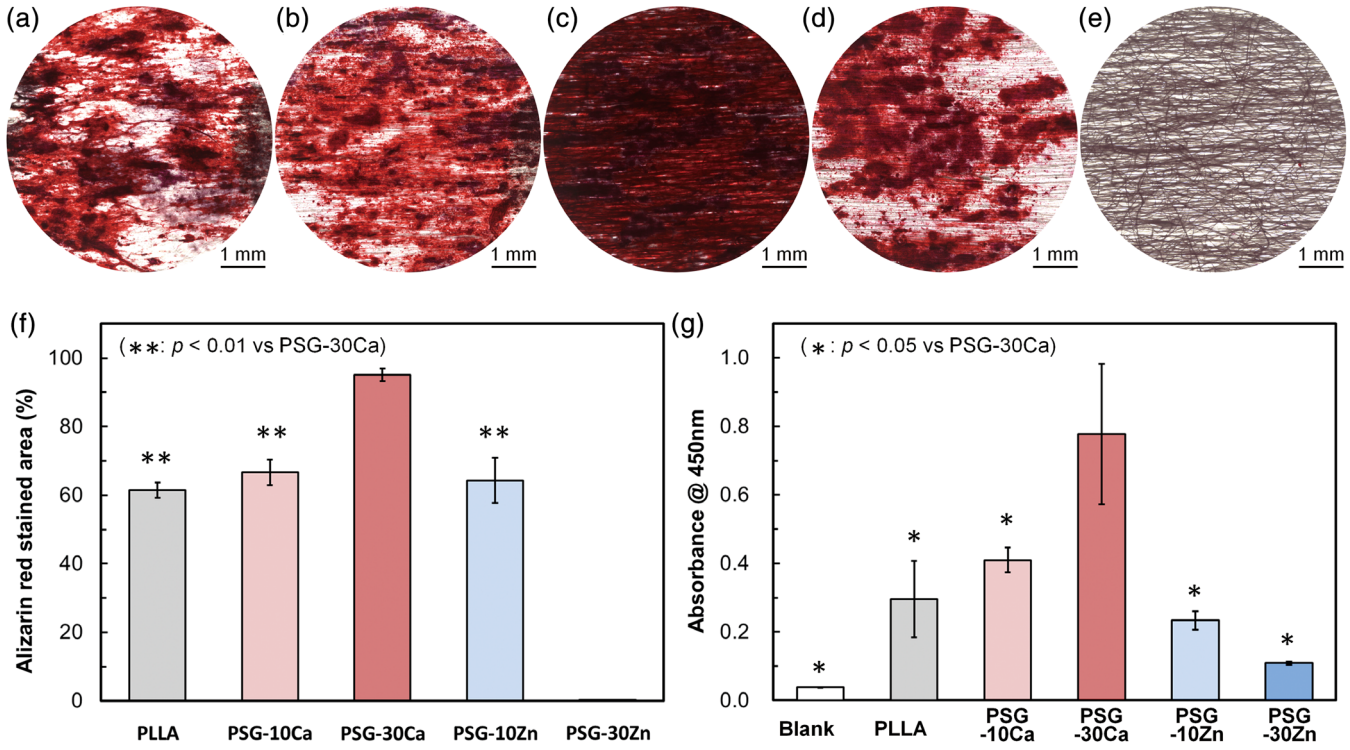

FIGURE 7 Alizarin red S staining images (φ 6 mm at center) of (a) PLLA, (b) PSG-10Ca, (c) PSG-30Ca, (d) PSG-10Zn, and (e) PSG-30Zn. (f) The stained area (red colored) ratio of the anisotropic scaffolds. (g) Absorbance at 450 nm of extracted Alizarin red dye from the anisotropic scaffolds. Error bars represent the standard deviation

orientation angles were distributed about a center of zero. The fiber diameters of PSG-30Ca and PSG-30Zn were larger than those of PLLA, PSG-10Ca, and PSG-10Zn, as shown in Figure 3f. *FD* showed no significant difference between the samples, as shown in Figure 3l.

The ion-releasing behaviors of the scaffolds are shown in Figure 4a,b. The release of silicate and Mg^{2+} ions from PSG-*x*Ca and PSG-*x*Zn increased with increasing soaking time. The amount of phosphate ions released from PSG-10Ca and PSG-*x*Zn increased, whereas that of PSG-30Ca was approximately constant. The release of Ca^{2+} and Zn^{2+} ions from PSG-10Ca and PSG-10Zn, respectively, increased with increasing soaking time. However, the amounts from PSG-30Ca and PSG-30Zn decreased. The XRD patterns of PSG-*x*Ca and PSG-*x*Zn are shown in Figure 4c. PSG-30Ca and PSG-30Zn showed peaks corresponding to hydroxyapatite (HAp, $Ca_{10}(PO_4)_6(OH)_2$, ICCD card: 74-0566) and hopeite ($Zn_3(PO_4)_2(H_2O)_4$, ICDD card: 76-0896), respectively, whereas PSG-10Ca and PSG-10Zn showed halo peaks.

3.3 | Osteoblast behavior on anisotropic scaffolds

The number of cells on PSG-*x*Ca and PSG-*x*Zn is shown in Figure 5. The cell numbers on PSG-*x*Ca and PSG-*x*Zn were significantly larger than those on PLLA at days 3 and 6. The fluorescence images of primary osteoblasts and cell orientation angle histograms are shown in Figure 6a–e,f–j, respectively. The cells adhered to the single fiber surfaces. In addition, the cells were aligned in the fiber-oriented direction (i.e., the collector rotation direction). PSG-30Zn showed fewer primary osteoblasts than the other scaffolds. The orientation angles of the cells were distributed about a center of zero. *CD* of PLLA, PSG-*x*Ca, and PSG-10Zn exhibited values greater than 0.85, whereas that of PSG-30Zn was 0.70, as shown in Figure 6k.

Alizarin red S staining was performed to visualize mineralization, as shown in Figure 7a–e. PSG-30Ca stained the whole area, and PLLA, PSG-10Ca, and PSG-10Zn were partially stained, whereas PSG-30Zn showed no staining. The stained area ratios of the scaffolds after culturing for 6 weeks are shown in Figure 7f. The stained area of PSG-30Ca was significantly larger than that of the others. Additionally, the absorbance of the extracted Alizarin red dye is presented in Figure 7g. The absorbance of PSG-30Ca was significantly larger than that of the others. The absorbance of PSG-30Zn was 0.11. The blank indicated the absorbance of the extract solution (5% formic acid), with a value of 0.04. The absorbance values of PLLA, PSG-10Ca, and PSG-10Zn cultured for 6 weeks without cells were the same as the blank, and those of PSG-30Ca and PSG-30Zn were approximately 0.1.

Preferential orientation of BAp *c*-axis evaluated by micro-XRD system and schematic illustration of analysis are depicted in Figure 8a. Micro-XRD patterns of the scaffolds after cultivation for 6 weeks with primary osteoblasts are shown in Figure 8b. PLLA, PSG-*x*Ca, and PSG-10Zn displayed peaks corresponding to HAp, whereas PSG-30Zn had a halo peak. The scaffolds cultivated for 6 weeks without cells also featured a halo peak. The obtained XRD patterns were fit to a Gaussian function. The dotted lines indicate reconstructed peaks of PSG-10Zn as

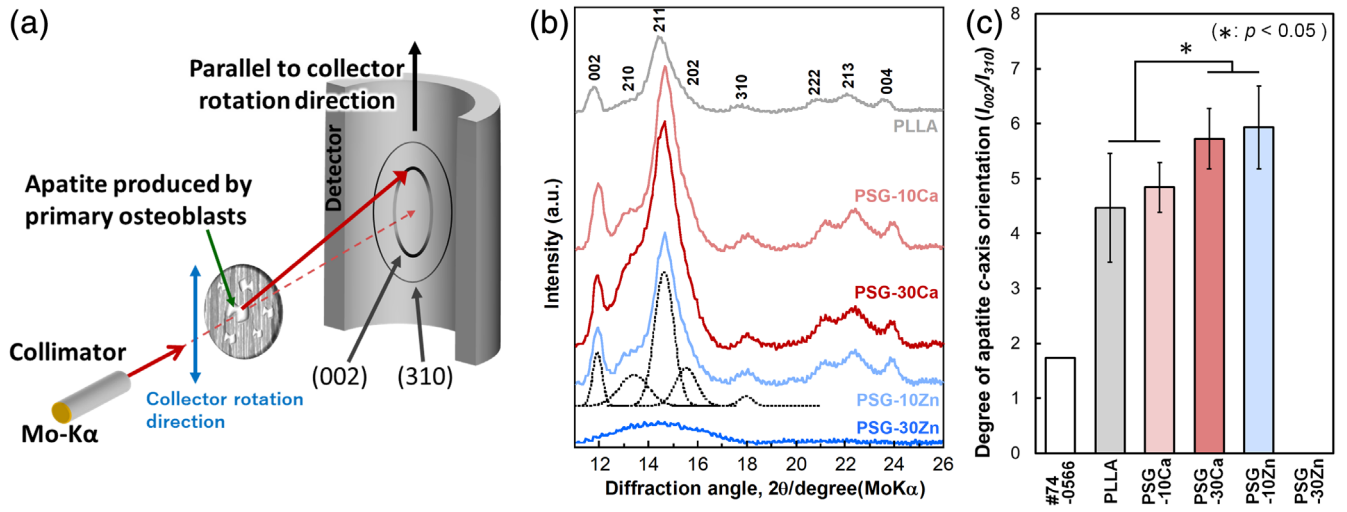

FIGURE 8 (a) Schematic illustration of the analysis of apatite orientation using transmission micro-XRD system. Reproduced from Ref. 41 with permission from the Royal Society of Chemistry. (b) Micro-XRD patterns of deposited minerals on anisotropic scaffolds. Dotted lines represent the Gaussian curves fitted to the patterns for PSG-10Zn. (c) Integrated intensity ratio of 002/310, that is, degree of apatite *c*-axis orientation, along the collector rotation direction. Error bars represent the standard deviation

a representative example. The degree of the apatite *c*-axis orientation (I_{002}/I_{310}) is shown in Figure 8c. The values of PLLA, PSG-xCa, and PSG-10Zn were larger than those of the reference (ICCD card: 74-0566; mineral hydroxyapatite from Holly Springs[55]). PSG-10Zn and PSG-30Ca showed significantly larger values than those of PLLA and PSG-10Ca.

4 | DISCUSSION

4.1 | Structures and properties of orthophosphosilicate glasses

The ^{31}P and ^{29}Si MAS-NMR spectra of PSG-Ca and PSG-Zn had symmetric peaks corresponding to the sole components, Q_p^0 and Q_{Si}^0, respectively. The ^{29}Si MAS-NMR spectrum of PSG-Zn indicated the possibility of the existence of the Q_{Si}^1 group, as evident by shoulders. However, Raman spectra showed no bands corresponding to the Q_{Si}^1 group, and the simulated spectrum of Q_{Si}^0 fit well with a single Gaussian peak assumption. The shoulders of PSG-Zn can be spinning side bands due to its broad spectrum compared with PSG-Ca. Accordingly, the silicate groups in PSG-Zn could conceivably be composed predominantly of Q_{Si}^0. The Raman band corresponding to the bending mode of phosphate chains with cation modifiers (230–350 cm^{-1})[51] was not observed in PSG-Ca and PSG-Zn, indicating that the glasses did not contain either pyro- or metaphosphate groups. In addition, the Raman bands assigned to the coupled vibration of P–O and Si–O stretching in P–O–Si bonds (1,180 and 800 cm^{-1})[56] were not observed in PSG-Ca and PSG-Zn. Moreover, the peak at −215 ppm in the ^{29}Si MAS-NMR spectra of PSG-Ca and PSG-Zn was not observed, which corresponds to the SiO_6 octahedra[57] that are able to form P–O–Si bonds.[58] These results suggest the absence of P–O–P, Si–O–Si, and P–O–Si bonds in PSG-Ca and PSG-Zn. Thus, the glasses did not contain long chain structures.

In general, invert glass consists of glass-forming tetrahedra and modifier ions linked through nonbridging oxygen atoms.[59] Mg^{2+} and Zn^{2+} can be classified as intermediate ions,[60] and in the glass they can act either as network modifiers (creating nonbridging oxygen) or network former (reducing nonbridging oxygen owing to the formation of MgO_4^{2-} or ZnO_4^{2-} tetrahedra).[61,62] In phosphate glasses, Mg^{2+} and Zn^{2+} ions can enter phosphate chain structures when the ions are present at high contents.[62–64] Similarly, Mg^{2+} and Zn^{2+} ions in silicate and phosphosilicate glasses enter the silicate network and form Si–O–Mg/Zn bonds.[65,66]

From the molecular dynamics simulation results, 90% of the Mg^{2+} ions in Na_2O–CaO–MgO–SiO_2 glasses were in the form of MgO_4^{2-} tetrahedra, and exhibited a role as a network former.[67] In the case of SiO_2–Na_2O–CaO–MgO–P_2O_5 glasses, Mg^{2+} ions were distributed in the silica-rich region, and the ion preferred to form MgO_4^{2-} tetrahedra with increasing MgO content.[68] Watts et al. reported that Mg^{2+} ions prefer to be in the silicate phase and remove modifying ions.[64] According to Karakassides et al., Mg^{2+} ions prefer to bridge with oxygen not belonging to PO_4 tetrahedra, whereas Ca^{2+} ions are more inclined to link with oxygen belonging to PO_4 tetrahedra.[51] Thus, Mg^{2+} ions in PSG-Ca/Zn preferentially form a Si–O–Mg bond as a network former in the form of MgO_4^{2-} tetrahedra.

Goel et al. reported that Mg^{2+} and Zn^{2+} ions in CaO–MgO–ZnO–P_2O_5–SiO_2–CaF_2 glasses exhibited similar structural features, and Zn^{2+} ions coordinated to the phosphate group rather than the silicate group.[69] Additionally, Zn^{2+} ions showed a stronger preference for phosphate groups than Mg^{2+} ions in high-ZnO content glass.[69] According to Montagne et al., Zn^{2+} ions in ZnO–Na_2O–P_2O_5 glasses were in the form of ZnO_4^{2-} tetrahedra, and preferentially bonded to Q_p^0 groups.[70] Thus, Zn^{2+} ions in PSG-Zn preferentially form a P–O–Zn bond as a network former in the form of ZnO_4^{2-} tetrahedra. Ca^{2+} ions in phosphosilicate glasses exhibited greater chemical affinity to phosphate ions than Mg^{2+} ions. Moreover, Ca^{2+} ions prefer to link

with oxygen belonging to PO_4 tetrahedra than with Mg^{2+} ions.[51] As a result, Ca^{2+} ions in PSG-Ca bond with phosphate groups to form P–O–Ca bonds.

In brief, Mg^{2+} ions in PSG-Ca/Zn preferentially form a Si–O–Mg bond, and Ca^{2+} and Zn^{2+} ions form P–O–Ca and P–O–Zn bonds, respectively. In particular, Mg^{2+} and Zn^{2+} ions entered the glass network structure as network formers in the form of MgO_4^{2-}/ZnO_4^{2-} tetrahedra. Consequently, the cumulative network-forming ability of Mg^{2+} and Zn^{2+} ions in PSG-Ca/Zn could explain why only Q_p^0 and Q_{Si}^0 groups were present.

The dissolution behavior of PSG-Ca was discussed in our previous work.[37] In brief, Mg^{2+} and Ca^{2+} ions in PSG-Ca preferentially formed Si–O–Mg and P–O–Ca bonds, respectively. The fundamental difference between silicate (SiO_4^{4-}) and phosphate (PO_4^{3-}) tetrahedra is that silicate has four single Si–O bonds, while phosphate has three single P–O bonds and a double P=O bond. Phosphate tetrahedra are preferentially attacked by water molecules in aqueous solutions because of the comparably high acidity and the delocalized electron. Additionally, phosphate species in aqueous solution are stable, whereas silicate species are easily polymerized.[71,72] Thus, P–O–Ca bonds can dissolve more easily than Si–O–Mg bonds, resulting in Ca^{2+} and phosphate ions exhibiting a larger release amount than Mg^{2+} and silicate ions.

The release percentage of all components from PSG-Zn was smaller than that of PSG-Ca until day 5. Introducing Zn^{2+} ions into silicate and phosphosilicate glasses was reported to improve their chemical durability.[65,66,69,73] This was because ZnO_4^{2-} entered the silicate network to form Si–O–Zn bonds and significantly increased the silicate network polymerization. On the other hand, the chemical durability of ZnO-containing phosphate glasses varied the ZnO content and phosphate chain structure. In metaphosphate glasses, chemical durability improved or showed no significant difference with the addition of ZnO up to 5 mol%. However, it significantly decreased with further addition of ZnO up to 20 mol%.[74,75] ZnO in metaphosphate glass switch their role from network modifier to former when containing more than 5 mol%, and ZnO_4^{2-} tetrahedra (i.e., network former) enter phosphate chains. However, the bonding energy of the Zn–O bond is smaller than that of the P–O bond, and the chemical durability of the glasses decreased by entering ZnO_4^{2-} tetrahedra into phosphate chain.[74] In contrast, the chemical durability of ZnO-containing PIGs increased with increasing ZnO content.[76–78] The chemical durability of phosphate invert glass is comparably larger than that of metaphosphate glass because the glass contains large amounts of Q_p^0 and Q_p^1, which can delocalize the P=O group.[30,76,79] Additionally, the glass network structure of invert glasses is easily influenced by cations. Zn^{2+} ions can classify intermediates, and their field strength (0.49 valence/Å^2) is larger than that of network modifiers such as Ca^{2+} (0.33), Sr^{2+} (0.28), and Na^+ (0.19) ions.[60] Consequently, the substitution or addition of ZnO into phosphate invert glass can improve their glass network structure, thereby improving their chemical durability.[76,78] PSG-Zn composed network former (P_2O_5, SiO_2) and intermediates (MgO, ZnO), and its network structure may be stronger compared with PSG-Ca. As discussed previously, intermediates in PSG-Zn act as network formers and enter the glass network structure. Therefore, the glass substituted ZnO for CaO, that is, PSG-Zn, exhibited improved chemical durability compared with PSG-Ca, since Zn^{2+} ions have a larger field strength than Ca^{2+} ions. The ion-releasing behavior of silicate-Mg^{2+} ion pairs from PSG-Zn was similar, since Mg^{2+} ions preferentially bond with the silicate group, as discussed previously. In contrast, the ion-releasing behavior of the phosphate-Zn^{2+} ion pair from PSG-Zn was not similar, where phosphate and Zn^{2+} ions were 7 and 0%, respectively, at day 7. This originated from the precipitation of hopeite, which is an important phase in zinc phosphate bone cement[80] and reflects biocompatibility.[81]

The percentage of silicate-Mg^{2+} and phosphate-Ca^{2+} ion pairs from PSG-Ca/Zn and PSG-Ca were approximately 30 and 40%, respectively, at day 7, which are comparatively larger than those of previous phosphosilicate glasses (e.g., 13% on day 7[38]). Accordingly, PSG-Ca and PSG-Zn can be candidate inorganic–organic composites as a resource of therapeutic ions for bone formation based on their excellent ion-releasing ability.

4.2 | Morphology of anisotropic scaffolds

Polymer fibers fabricated via an electrospinning process are formed by the creation and elongation of an electric field fluid jet with a velocity of 0.5–5 m/s.[82] In this work, the collecting speed was set to 4.7 m/s and a single stable jet was formed during the process. Hence, the fibers were collected by a drum collector with stretching to the collector rotation direction. Accordingly, the fiber diameter can be estimated as follows[40]:

$$R = K_s \times 2\sqrt{\frac{F}{\pi v_c}}, \tag{5}$$

where, R is the diameter of the fiber (m), K_s is the shrinkage ratio of the fiber, F is the flow rate of the electrospinning solution (L/s), and v_c is the collecting speed (m/s). The diameter, R, was estimated to be 26 μm under the assumption of K_s = 1.0, which indicates that the fiber did not shrink. The fiber diameter of PLLA was 7.6 μm and K_{s_PLLA} was calculated as 0.29. The estimated $K_{s.est}$ for the scaffolds was calculated as follows:

$$K_{s.est} = \frac{(100-x)K_{s\_PLLA} + xK_{s\_glass}}{100}, \tag{6}$$

where, x is vol% of PSG-Ca/Zn contained in the scaffolds. K_{s_PLLA} is 0.29 as calculated previously, and K_{s_glass} is 1, which does not dissolve or swell by chloroform. Accordingly, $K_{s.est}$ of PSG-10Ca/Zn and PSG-30Ca/Zn were 0.36 and 0.50, respectively. Finally, the calculated R values of PSG-10Ca/Zn and PSG-30Ca/Zn were 9.4 and 13 μm, respectively. The measured diameter of PSG-10Ca/Zn and PSG-30Ca/Zn was 9.8 ± 3.9 and 16.0 ± 7.1 μm, respectively, which agreed well with the calculated R. In our previous work, scaffolds with a fiber diameter greater than 10 μm showed a strong positive correlation

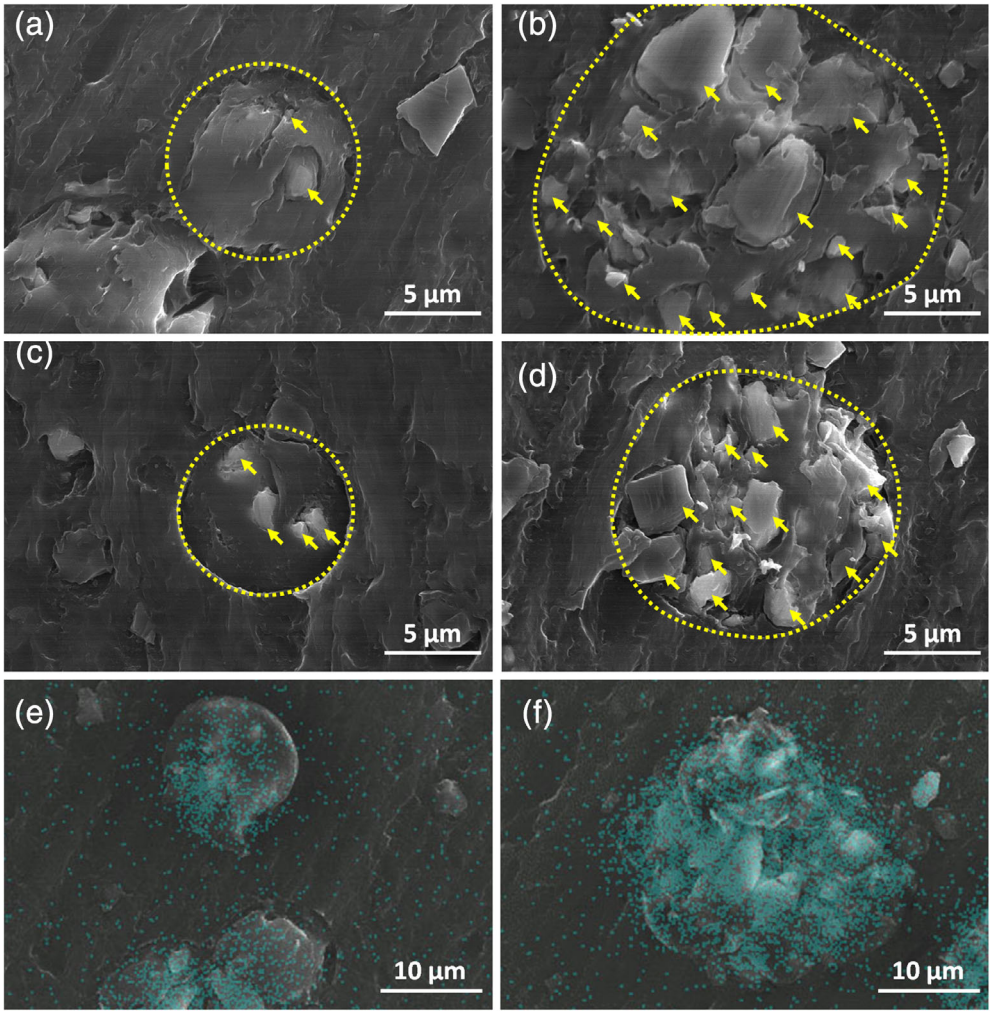

FIGURE 9 Cross section SEM images of (a) PSG-10Ca, (b) PSG-30Ca, (c) PSG-10Zn, and (d) PSG-30Zn. Dotted line indicates boundary of fiber and epoxy resin. The yellow arrows point glass powders. SEM–EDX mapping images of (e) PSG-10Ca and (f) PSG-30Ca. Light-blue dots represent detected Ca element

between *FD* and *CD*.[40] The diameter of the fiber in scaffolds was approximately greater than 10 μm, and the cell adhered to a single fiber.[42] Thus, cell alignment on the scaffolds can be controlled by their morphology. The morphology of PSG-*x*Ca/Zn was well controlled with an anisotropic shape, of which the *FD*s were approximately 0.9, and the value was suitable for controlling cell alignment in one direction.

PSG-30Ca/Zn exhibited dissolution behavior similar to that of glass powder, whereas all components from PSG-10Ca/Zn were released at approximately the same percentage. This originated from the amount of glass powder content in the scaffolds. Cross-sectional views of PSG-*x*Ca and PSG-*x*Zn are shown in Figure 9a–d, and the Ca element mapping images of PSG-*x*Ca are shown in Figure 9e,f. Glass powders in PSG-30Ca/Zn dispersed homogeneously in the fiber, and connected each other, which was found in the percolative composite.[83] This was also found in the Ca element mapping image (Figure 9f). In contrast, glass powders in PSG-10Ca/Zn are not connected to each other. As a result, the powders existing near the surface of the fiber can release ions. Consequently, the scaffolds containing 30 vol% of glass powders exhibited similar ion-releasing behavior with the glass powders, since the aqueous solution is accessible to the powders. Ion-release behavior of the scaffolds containing 10 vol% of glass powders was influenced by the glass network structure and also by the position in the fiber. As a result, the scaffolds showed sustained release behavior. The scaffolds with 30 vol% of glass powders showed precipitation of HAp and hopeite on PSG-30Ca and PSG-30Zn, respectively, due to the excellent ion-release ability. PSG-30Ca showed HAp precipitation due to the carboxyl group in PLLA, which induces nucleation of HAp,[84] whereas PSG-Ca (glass powder) did not show any precipitation. PSG-30Zn showed precipitation of hopeite similar to PSG-Zn (glass powder). Thus, the ion-releasing behavior of the scaffolds can be manipulated by the glass network structure and also by the content of the glass powder, which determines the position of the particles in the fiber.

4.3 | Osteoblast behavior and calcified tissues on anisotropic scaffolds

The cell numbers on PSG-*x*Ca/Zn were significantly larger than those on PLLA. This was caused by the dissolved silicate and Mg^{2+} ions from the scaffolds, which improved MC3T3-E1 cell adhesion and proliferation.[16,19] A negative effect of Zn^{2+} ions on MC3T3-E1 cells was not observed. Calcification of tissues by the primary osteoblasts, which stained red, was observed in PLLA, PSG-xCa, and PSG-10Zn.

However, PSG-30Zn showed no calcified tissues with Alizarin red S staining, and the absorbance of Alizarin red-extracted solution was almost the same as culturing without cells, which indicates that Alizarin red S stain attached to bivalent species, that is, glass particles. In addition, PSG-30Zn exhibited a halo peak in the micro-XRD analysis, similar to the scaffolds cultivated without cells, which indicates that no crystalline precipitation occurred. Zn^{2+} ions have been reported to show mild cytotoxicity in healthy tissues.[85] According to Aina et al., Zn^{2+} ions from phosphosilicate glass showed cytotoxicity for human osteoblasts (MG-63), and the cells released lactate dehydrogenase (index of cytotoxicity) and were damaged via oxidative stress.[86] Similarly, zinc-containing phosphate glasses showed a negative effect on MG-63 cells.[74,87] However, human-derived osteosarcoma cells (Saos-2) on ZnO-containing phosphate invert glass film, which has excellent chemical durability,[78] exhibited no cytotoxicity.[88] The ALP activity of MG-63 cells on metaphosphate glasses with 5 mol% of ZnO was improved by released Zn^{2+} ions.[74] In the case of phosphosilicate glasses with 5 mol% ZnO, Zn^{2+} ions from the glasses enhanced endothelial cells (BAE-1) spreading, and exhibited significantly larger cell numbers compared with the glass without ZnO.[73] Thus, manipulation of Zn^{2+} ion release in small amounts can be effective for promoting cell functions. The amount of Zn^{2+} ions released from PSG-30Zn might be cytotoxic to primary osteoblasts, whereas MC3T3-E1 cells showed no cytotoxicity. This may be due to the sensitivity of cells to Zn^{2+} ions.

In cell culture tests, PSG-10Ca/Zn exhibited enhanced cell adhesion and proliferation. However, no significant enhancement of calcification was observed. This reflected the amount of glass powder content in the scaffolds, as discussed previously; 10 vol% of the glass powder cannot be connected to each other in the composite as shown in Figure 9a,c,e. As a result, the powders existing near the surface of the fiber can release ions. However, the amount may not be sufficient for enhancing calcification. PSG-30Ca exhibited significantly larger calcified tissue area and absorbance of Alizarin red-extracted solution than the others. PSG-30Ca contained 30 vol% of powders in a PLLA matrix, and the powders connected with each other, that is, percolative composite,[83] as shown in Figure 9b,f. Thus, PSG-30Ca can release more therapeutic ions, such as silicate, phosphate, Ca^{2+}, and Mg^{2+} ions, and are expected to stimulate bone formation (bone quantity).

Primary osteoblasts on PLLA, PSG-*x*Ca, and PSG-10Zn were attached to a single fiber and elongated in the fiber longitude direction, which was similar to the results of our previous work.[39,40] Moreover, their *CD* values were larger than 0.85, indicating successful control of cell alignment by morphology of the scaffolds. PSG-30Zn, however, exhibited a smaller *CD* value than the others, as some cells were not stretched and had a round shape. This originated from the mild cytotoxicity of Zn^{2+} ions for primary osteoblasts, such that PSG-30Zn featured fewer cells on the scaffold compared with others. In our previous work, aligned primary osteoblasts produced the collagen matrix in the direction of cellular alignment. Moreover, the *c*-axis of the apatite crystals produced by primary osteoblasts indicated preferential alignment along the direction of the collagen matrix.[6] The degrees of the apatite *c*-axis orientation on PLLA, PSG-*x*Ca, and PSG-10Zn were larger than the reference data. BAp *c*-axis orientation degree on random-aligned PLLA scaffold was approximately 3.5 in our previous work.[41] The values in the present scaffolds are 4.5–6. Thus, the morphological design of the scaffolds in this work was successfully controlled by cell alignment and direction of calcification ("bone quality").

PSG-30Ca and PSG-10Zn exhibited significantly larger degrees of *c*-axis orientation compared with PLLA and PSG-10Ca. Moriishi et al. reported that OCN, which is a noncollagenous protein in bone, is necessary for the formation of higher bone quality and strength by adjusting the *c*-axis orientation of BAp parallel to collagen fibrils, but is not involved in the regulation of bone quantity.[89] Silicate and Ca^{2+} ions have been reported to upregulate OCN in human osteoblasts.[17] Zn^{2+} ions also stimulate OCN in rat bone marrow mesenchymal stem cells[21] and MC3T3-E1.[22] Specifically, 50–100 μM Zn^{2+} ions upregulate OCN mRNA expression level by 3.5-fold.[22] The larger *c*-axis orientation degrees of PSG-30Ca and PSG-10Zn may be influenced by the OCN expression level due to the released ions from the scaffolds, although the *FD*s of PLLA, PSG-*x*Ca, and PSG-*x*Zn were similar. As discussed previously, PSG-30Ca exhibits excellent ion releasability, and enhances osteoblasts proliferation and calcification, whereas the ability of PSG-10Ca was not enough for enhancement of bone formation. Hence, the larger *c*-axis orientation degree of PSG-30Ca than PSG-10Ca may originate from silicate and Ca^{2+} ion releasability, which can upregulate OCN. The amount of Zn^{2+} ions released from PSG-10Zn into the TBS was approximately 45 μM at day 12, which can upregulate OCN. As a result, the *c*-axis orientation degree was larger than that of PLLA and PSG-10Ca. Therefore, PSG-30Ca is implicated as a candidate scaffold with simultaneous reconstruction of bone quality and bone quantity because of its' excellent ion-release behavior and morphology for manipulation of cell alignment.

5 | CONCLUSION

Novel anisotropic scaffolds for the simultaneous reconstruction of bone quality and quantity were established. PSGs demonstrated excellent ion-releasing ability owing to the unique glass network structure without a long chain structure. Such an ability is appropriate as a resource of therapeutic ions for the stimulation of bone formation. The scaffold morphology was designed to create strong cell alignment by the fiber diameter and orientation. PSG-30Ca promotes cell adhesion, proliferation, and calcification owing to the released ions from the glass. Moreover, cell alignment and direction of calcification on PSG-30Ca were successfully manipulated by designing the morphology of the scaffolds. The obtained results indicate that the fabricated scaffolds could regulate the arrangement of osteoblasts and the direction of calcification according to morphology (bone quality), and that the released ions improve bone formation (bone quantity). These findings could inform important developments and a new strategy for in situ bone regeneration with simultaneous reconstruction of bone quality and quantity.

ACKNOWLEDGMENTS

This work was supported in part by JSPS KAKENHI grant numbers 18H05254 and 17H06224.

CONFLICT OF INTEREST

The authors declare no conflicts of interest.

ORCID

Sungho Lee https://orcid.org/0000-0002-4367-9573
Fukue Nagata https://orcid.org/0000-0002-5284-9626
Katsuya Kato https://orcid.org/0000-0001-8981-8359
Toshihiro Kasuga https://orcid.org/0000-0002-8745-8932
Takayoshi Nakano https://orcid.org/0000-0001-8052-1698

REFERENCES

1. Weiner, S., & Wagner, H. D. (1998). The material bone: structure-mechanical function relations. *Annu Rev Mater Sci*, *28*, 271–298.
2. Seto, J., Gupta, H. S., Zaslansky, P., Wagner, H. D., & Fratzl, P. (2008). Tough lessons from bone: extreme mechanical anisotropy at the mesoscale. *Adv Funct Mater*, *18*, 1905–1911.
3. Nakano, T., Kaibara, K., Tabata, Y., Nagata, N., Enomoto, S., Marukawa, E., & Umakoshi, Y. (2002). Unique alignment and texture of biological apatite crystallites in typical calcified tissues analyzed by microbeam x-ray diffractometer system. *Bone*, *31*, 479–487.
4. Ishimoto, T., Nakano, T., Umakoshi, Y., Yamamoto, M., & Tabata, Y. (2013). Degree of biological apatite *c*-axis orientation rather than bone mineral density controls mechanical function in bone regenerated using recombinant bone morphogenetic protein-2. *J Bone Miner Res*, *28*, 1170–1179.
5. Nakano, T., Kaibara, K., Ishimoto, T., Tabata, Y., & Umakoshi, Y. (2012). Biological apatite (BAp) crystallographic orientation and texture as a new index for assessing the microstructure and function of bone regenerated by tissue engineering. *Bone*, *51*, 741–747.
6. Matsugaki, A., Isobe, Y., Saku, T., & Nakano, T. (2015). Quantitative regulation of bone-mimetic, oriented collagen/apatite matrix structure depends on the degree of osteoblast alignment on oriented collagen substrates. *J Biomed Mater Res A*, *103*, 489–499.
7. Matsugaki, A., Aramoto, G., & Nakano, T. (2012). The alignment of MC3T3-E1 osteoblasts on steps of slip traces introduced by dislocation motion. *Biomaterials*, *33*, 7327–7335.
8. Nakanishi, Y., Matsugaki, A., Kawahara, K., Ninomiya, T., Sawada, H., & Nakano, T. (2019). Unique arrangement of bone matrix orthogonal to osteoblast alignment controlled by Tspan11-mediated focal adhesion assembly. *Biomaterials*, *209*, 103–110.
9. Pham, Q. P., Sharma, U., & Mikos, D. A. G. (2006). Electrospinning of polymeric nanofibers for tissue engineering applications: a review. *Tissue Eng*, *12*, 1197–1211.
10. Murugan, R., & Ramakrishna, S. (2006). Nano-featured scaffolds for tissue engineering: a review of spinning methodologies. *Tissue Eng*, *12*, 435–447.
11. Lee, J.-h., Lee, Y. J., H-j, C., & Shin, H. (2013). Guidance of in vitro migration of human mesenchymal stem cells and in vivo guided bone regeneration using aligned electrospun fibers. *Tissue Eng Part A*, *20*, 2031–2042.
12. Madhurakkat Perikamana, S. K., Lee, J., Ahmad, T., Jeong, Y., Kim, D.-G., Kim, K., & Shin, H. (2015). Effects of immobilized BMP-2 and nanofiber morphology on in vitro osteogenic differentiation of hMSCs and in vivo collagen assembly of regenerated bone. *ACS Appl Mater Interfaces*, *7*, 8798–8808.
13. Hench, L. L. (1998). Bioceramics. *J Am Ceram Soc*, *81*, 1705–1728.
14. Hench, L. L. (2006). The story of bioglass. *J Mater Sci Mater Med*, *17*, 967–978.
15. Hoppe, A., Güldal, N. S., & Boccaccini, A. R. (2011). A review of the biological response to ionic dissolution products from bioactive glasses and glass-ceramics. *Biomaterials*, *32*, 2757–2774.
16. Xynos, I. D., Edgar, A. J., Buttery, L. D. K., Hench, L. L., & Polak, J. M. (2000). Ionic products of bioactive glass dissolution increase proliferation of human osteoblasts and induce insulin-like growth factor II mRNA expression and protein synthesis. *Biochem Biophys Res Commun*, *276*, 461–465.
17. Xynos, I. D., Hukkanen, J. M. V., Batten, J. J., Buttery, D. L., Hench, L. L., & Polak, M. J. (2000). Bioglass 45S5 stimulates osteoblast turnover and enhances bone formation in vitro: implications and applications for bone tissue engineering. *Calcif Tissue Int*, *67*, 321–329.
18. Julien, M., Khoshniat, S., Lacreusette, A., Gatius, M., Bozec, A., Wagner, E. F., et al. (2009). Phosphate-dependent regulation of MGP in osteoblasts: role of ERK1/2 and Fra-1. *J Bone Miner Res*, *24*, 1856–1868.
19. Yamada, S., Ota, Y., Obata, A., & Kasuga, T. (2017). Osteoblast-like cell responses to ion products released from magnesium- and silicate-containing calcium carbonates. *Biomed Mater Eng*, *28*, 47–56.
20. Hall, S. L., Dimai, H. P., & Farley, J. R. (1999). Effects of zinc on human skeletal alkaline phosphatase activity in vitro. *Calcif Tissue Int*, *64*, 163–172.
21. Oh, S.-A., Won, J.-E., & Kim, H.-W. (2011). Composite membranes of poly(lactic acid) with zinc-added bioactive glass as a guiding matrix for osteogenic. *J Biomater Appl*, *27*(4), 413–422.
22. Wu, X., Itoh, N., Taniguchi, T., Nakanishi, T., Tatsu, Y., Yumoto, N., & Tanaka, K. (2003). Zinc-induced sodium-dependent vitamin C transporter 2 expression: potent roles in osteoblast differentiation. *Arch Biochem Biophys*, *420*, 114–120.
23. Kwun, I.-S., Cho, Y.-E., Lomeda, R.-A. R., Shin, H.-I., Choi, J.-Y., Kang, Y.-H., & Beattie, J. H. (2010). Zinc deficiency suppresses matrix mineralization and retards osteogenesis transiently with catch-up possibly through Runx 2 modulation. *Bone*, *46*, 732–741.
24. Marie, P. J. (2010). The calcium-sensing receptor in bone cells: a potential therapeutic target in osteoporosis. *Bone*, *46*, 571–576.
25. Maeno, S., Niki, Y., Matsumoto, H., Morioka, H., Yatabe, T., Funayama, A., … Tanaka, J. (2005). The effect of calcium ion concentration on osteoblast viability, proliferation and differentiation in monolayer and 3D culture. *Biomaterials*, *26*, 4847–4855.
26. Kasuga, T., & Abe, Y. (1999). Calcium phosphate invert glasses with soda and titania. *J Non-Cryst Solids*, *243*, 70–74.
27. Lee, S., Obata, A., & Kasuga, T. (2009). Ion release from SrO-CaO-TiO_2-P_2O_5 glasses in Tris buffer solution. *J Cerma Soc Jpn*, *117*, 935–938.
28. Maeda, H., Lee, S., Miyajima, T., Obata, A., Ueda, K., Narushima, T., & Kasuga, T. (2016). Structure and physicochemical properties of CaO–P_2O_5–Nb_2O_5–Na_2O glasses. *J Non-Cryst Solids*, *432*, 60–64.
29. Lee, S. (2020). Development of glass-related biomaterials for enhanced bone regeneration via stimulation of cell function. *J Ceram Soc Jpn*, *128*, 349–356.
30. Lee, S., Maeda, H., Obata, A., Ueda, K., Narushima, T., & Kasuga, T. (2015). Structures and dissolution behaviors of CaO-P_2O5-TiO_2/Nb_2O_5 (ca/P ≥ 1) invert glasses. *J Non-Cryst Solids*, *426*, 35–42.
31. Lee, S., Maeda, H., Obata, A., Ueda, K., Narushima, T., & Kasuga, T. (2015). Structure and dissolution behavior of MgO-P_2O_5-TiO_2/Nb_2O_5 (mg/P ≥ 1) invert glasses. *J Ceram Soc Jpn*, *123*, 942–948.
32. Lee, S., Maeda, H., Obata, A., Ueda, K., Narushima, T., & Kasuga, T. (2016). Structures and dissolution behaviors of MgO–CaO–P_2O_5–Nb_2O_5 glasses. *J Non-Cryst Solids*, *438*, 18–25.
33. Obata, A., Takahashi, Y., Miyajima, T., Ueda, K., Narushima, T., & Kasuga, T. (2012). Effects of niobium ions released from calcium phosphate invert glasses containing Nb_2O_5 on osteoblast-like cell functions. *ACS Appl Mater Interfaces*, *4*, 5684–5690.
34. Lee, S., Obata, A., Brauer, D. S., & Kasuga, T. (2015). Dissolution behavior and cell compatibility of alkali-free MgO-CaO-SrO-TiO_2-P_2O_5 glasses for biomedical applications. *Biomed Glasses*, *1*, 151–158.

35. Kasuga, T., Hattori, T., & Niinomi, M. (2012). Phosphate glasses and glass-ceramics for biomedical applications. *Phosphorus Res Bull*, *26*, 8–15.
36. Lee, S., Maçon, A. L. B., & Kasuga, T. (2016). Structure and dissolution behavior of orthophosphate MgO–CaO–P_2O_5–Nb_2O_5 glass and glass-ceramic. *Mater Lett*, *175*, 135–138.
37. Lee, S., Nakano, T., & Kasuga, T. (2017). Formation and structural analysis of 15MgO–15CaO–8P_2O_5–4SiO_2 glass. *J Non-Cryst Solids*, *457*, 73–76.
38. Lee, S., Ueda, K., Narushima, T., Nakano, T., & Kasuga, T. (2017). Preparation of orthophosphate glasses in the MgO-CaO-SiO_2-Nb_2O_5-P_2O_5 system. *Biomed Mater Eng*, *28*, 23–30.
39. Lee, S., Matsugaki, A., Kasuga, T., & Nakano, T. (2019). Development of bifunctional oriented bioactive glass/poly(lactic acid) composite scaffolds to control osteoblast alignment and proliferation. *J Biomed Mater Res A*, *107*, 1031–1041.
40. Lee, S., Kiyokane, Y., Kasuga, T., & Nakano, T. (2019). Oriented siloxane-containing vaterite/poly(lactic acid) composite scaffolds for controlling osteoblast alignment and proliferation. *J Asian Ceram Soc*, *7*, 228–237.
41. Lee, S., Nagata, F., Kato, K., & Nakano, T. (2020). Bone apatite anisotropic structure control via designing fibrous scaffolds. *RSC Adv*, *10*, 13500–13506.
42. Sun, T., Norton, D., McKean, R. J., Haycock, J. W., Ryan, A. J., & MacNeil, S. (2007). Development of a 3D cell culture system for investigating cell interactions with electrospun fibers. *Biotechnol Bioeng*, *97*, 1318–1328.
43. Matsugaki, A., Fujiwara, N., & Nakano, T. (2013). Continuous cyclic stretch induces osteoblast alignment and formation of anisotropic collagen fiber matrix. *Acta Biomater*, *9*, 7227–7235.
44. Lee, S., Nakano, T., & Kasuga, T. (2017). Structure, dissolution behavior, cytocompatibility, and antibacterial activity of silver-containing calcium phosphate invert glasses. *J Biomed Mater Res A*, *105*, 3127–3135.
45. Wong, G., & Cohn, D. V. (1974). Separation of parathyroid hormone and calcitonin-sensitive cells from non-responsive bone cells. *Nature*, *252*, 713–715.
46. Matsugaki, A., Aramoto, G., Ninomiya, T., Sawada, H., Hata, S., & Nakano, T. (2015). Abnormal arrangement of a collagen/apatite extracellular matrix orthogonal to osteoblast alignment is constructed by a nanoscale periodic surface structure. *Biomaterials*, *37*, 134–143.
47. Miyazaki, T., Miyauchi, S., Tawada, A., Anada, T., Matsuzaka, S., & Suzuki, O. (2008). Oversulfated chondroitin sulfate-E binds to BMP-4 and enhances osteoblast differentiation. *J Cell Physiol*, *217*, 769–777.
48. Ishimoto, T., Sato, B., Lee, J.-W., & Nakano, T. (2017). Co-deteriorations of anisotropic extracellular matrix arrangement and intrinsic mechanical property in c-src deficient osteopetrotic mouse femur. *Bone*, *103*, 216–223.
49. Matsugaki, A., Harada, T., Kimura, Y., Sekita, A., & Nakano, T. (2018). Dynamic collision behavior between osteoblasts and tumor cells regulates the disordered arrangement of collagen fiber/apatite crystals in metastasized bone. *Int J Mol Sci*, *19*, 3474.
50. Umeno, A., Kotani, H., Iwasaka, M., & Ueno, S. (2001). Quantification of adherent cell orientation and morphology under strong magnetic fields. *IEEE Trans Magn*, *37*, 2909–2911.
51. Karakassides, M. A., Saranti, A., & Koutselas, I. (2004). Preparation and structural study of binary phosphate glasses with high calcium and/or magnesium content. *J Non-Cryst Solids*, *347*, 69–79.
52. Mysen, B. O., Virgo, D., & Scarfe, C. M. (1980). Relations between the anionic structure and viscosity of silicate melts – a Raman-spectroscopic study. *Am Mineral*, *65*, 690–710.
53. Sun, Y., Zhang, Z., Liu, L., & Wang, X. (2015). FTIR, Raman and NMR investigation of CaO–SiO_2–P_2O_5 and CaO–SiO_2–TiO_2–P_2O_5 glasses. *J Non-Cryst Solids*, *420*, 26–33.
54. Hansen, M. R., Jakobsen, H. J., & Skibsted, J. (2003). ^{29}Si chemical shift anisotropies in calcium silicates from high-field ^{29}Si MAS NMR spectroscopy. *Inorg Chem*, *42*, 2368–2377.
55. Sudarsanan, K., & Young, R. A. (1969). Significant precision in crystal structural details. Holly Springs hydroxyapatite. *Acta Crystallogr B*, *25*, 1534–1543.
56. Chakraborty, I. N., & Condrate, R. A. (1985). Vibrational spectra of glasses in the Na_2O-SiO_2-P_2O_5 system with a 1:1 SiO_2:P_2O_5 molar ratio. *Phys Chem Glasses*, *26*, 68–73.
57. Dupree, R., Holland, D., & Mortuza, M. G. (1988). Six-coordinated silicon in glasses. *Nature*, *328*, 416–417.
58. Ahsan, M. R., & Mortuza, M. G. (2005). Infrared spectra of xCaO(1 – x – z)SiO_2zP_2O_5 glasses. *J Non-Cryst Solids*, *351*, 2333–2340.
59. Brow, R. K. (2000). Review: the structure of simple phosphate glasses. *J Non-Cryst Solids*, *263–264*, 1–28.
60. Varshneya, A. K. (1994). Chapter 3 - Glass formation principles. In A. Varshneya & J. C. Mauro (Eds.), *Fundamentals of Inorganic Glasses* (pp. 27–59). San Diego, CA: Academic Press.
61. Brauer, D. S., Wilson, R. M., & Kasuga, T. (2012). Multicomponent phosphate invert glasses with improved processing. *J Non-Cryst Solids*, *358*, 1720–1723.
62. Cacciotti, I. (2017). Bivalent cationic ions doped bioactive glasses: the influence of magnesium, zinc, strontium and copper on the physical and biological properties. *J Mater Sci*, *52*, 8812–8831.
63. Shahrabi, S., Hesaraki, S., Moemeni, S., & Khorami, M. (2011). Structural discrepancies and in vitro nanoapatite formation ability of sol–gel derived glasses doped with different bone stimulator ions. *Ceram Int*, *37*, 2737–2746.
64. Watts, S. J., Hill, R. G., O'Donnell, M. D., & Law, R. V. (2010). Influence of magnesia on the structure and properties of bioactive glasses. *J Non-Cryst Solids*, *356*, 517–524.
65. Chen, X., Brauer, D. S., Karpukhina, N., Waite, R. D., Barry, M., McKay, I. J., & Hill, R. G. (2014). 'Smart' acid-degradable zinc-releasing silicate glasses. *Mater Lett*, *126*, 278–280.
66. Blochberger, M., Hupa, L., & Brauer Delia, S. (2015). Influence of zinc and magnesium substitution on ion release from bioglass 45S5 at physiological and acidic pH. *Biomed Glasses*, *1*, 51–69.
67. Pedone, A., Malavasi, G., Menziani, M. C., Segre, U., & Cormack, A. N. (2008). Role of magnesium in soda-lime glasses: insight into structural, transport, and mechanical properties through computer simulations. *J Phys Chem C*, *112*, 11034–11041.
68. Pedone, A., Malavasi, G., & Menziani, M. C. (2009). Computational insight into the effect of CaO/MgO substitution on the structural properties of phospho-silicate bioactive glasses. *J Phys Chem C*, *113*, 15723–15730.
69. Goel, A., Kapoor, S., Tilocca, A., Rajagopal, R. R., & Ferreira, J. M. F. (2013). Structural role of zinc in biodegradation of alkali-free bioactive glasses. *J Mater Chem B*, *1*, 3073–3082.
70. Montagne, L., Palavit, G., & Delaval, R. (1997). ^{31}P NMR in (100 - x)($NaPO_3$)-xZnO glasses. *J Non-Cryst Solids*, *215*, 1–10.
71. Abou Neel, E. A., Pickup, D. M., Valappil, S. P., Newport, R. J., & Knowles, J. C. (2009). Bioactive functional materials: a perspective on phosphate-based glasses. *J Mater Chem*, *19*, 690–701.
72. Sales, B. C., Boatner, L. A., & Ramey, J. O. (2000). Chromatographic studies of the structures of amorphous phosphates: a review. *J Non-Cryst Solids*, *263–264*, 155–166.
73. Aina, V., Malavasi, G., Fiorio Pla, A., Munaron, L., & Morterra, C. (2009). Zinc-containing bioactive glasses: surface reactivity and behaviour towards endothelial cells. *Acta Biomater*, *5*, 1211–1222.
74. Yunqi, W., Chenkai, Z., Andrew, P., Chris, R., Ifty, A., & Nusrat, S. (2019). Effects of ZnO addition on thermal properties, degradation and biocompatibility of $P_{45}Mg_{24}Ca_{16}Na_{(15-x)}Zn_x$ glasses. *Biomed Glasses*, *5*, 53–66.
75. Salih, V., Patel, A., & Knowles, J. C. (2007). Zinc-containing phosphate-based glasses for tissue engineering. *Biomed Mater*, *2*, 11–20.

76. Takebe, H., Baba, Y., & Kuwabara, M. (2006). Dissolution behavior of ZnO–P_2O_5 glasses in water. *J Non-Cryst Solids*, *352*, 3088–3094.
77. Chenu, S., Werner-Zwanziger, U., Calahoo, C., & Zwanziger, J. W. (2012). Structure and properties of $NaPO_3$–ZnO–Nb_2O_5–Al_2O_3 glasses. *J Non-Cryst Solids*, *358*, 1795–1805.
78. Lee, S., Uehara, H., Maçon, A. L. B., Maeda, H., Obata, A., Ueda, K., … Kasuga, T. (2016). Preparation of antibacterial ZnO-CaO-P_2O_5-Nb_2O_5 invert glasses. *Mater Trans*, *57*, 2072–2076.
79. Masai, H., Shirai, R., Yoshida, K., Takahashi, Y., Ihara, R., Fujiwara, T., … Yoko, T. (2013). ^{31}P NMR and IR study of highly water-stable SrO-BaO-Nb_2O_5-P_2O_5 glass and glass-ceramics. *Chem Lett*, *42*, 1305–1307.
80. Liu, B., Zhang, X., Xiao, G.-y., & Lu, Y.-p. (2015). Phosphate chemical conversion coatings on metallic substrates for biomedical application: a review. *Mater Sci Eng C*, *47*, 97–104.
81. Zhao, X.-c., Xiao, G.-y., Zhang, X., Wang, H.-y., & Lu, Y.-p. (2014). Ultrasonic induced rapid formation and crystal refinement of chemical conversed hopeite coating on titanium. *J Phys Chem C*, *118*, 1910–1918.
82. Reneker, D. H., & Yarin, A. L. (2008). Electrospinning jets and polymer nanofibers. *Polymer*, *49*, 2387–2425.
83. Yang, X., Hu, J., Chen, S., & He, J. (2016). Understanding the percolation characteristics of nonlinear composite dielectrics. *Sci Rep*, *6*, 30597.
84. Tanahashi, M., & Matsuda, T. (1997). Surface functional group dependence on apatite formation on self-assembled monolayers in a simulated body fluid. *J Biomed Mater Res*, *34*, 305–315.
85. Yamamoto, A., Honma, R., & Sumita, M. (1998). Cytotoxicity evaluation of 43 metal salts using murine fibroblasts and osteoblastic cells. *J Biomed Mater Res*, *39*, 331–340.
86. Aina, V., Perardi, A., Bergandi, L., Malavasi, G., Menabue, L., Morterra, C., & Ghigo, D. (2007). Cytotoxicity of zinc-containing bioactive glasses in contact with human osteoblasts. *Chem Biol Interact*, *167*, 207–218.
87. Abou Neel, E., O'Dell, L., Smith, M., & Knowles, J. (2008). Processing, characterisation, and biocompatibility of zinc modified metaphosphate based glasses for biomedical applications. *J Mater Sci Mater Med*, *19*, 1669–1679.
88. Sato, P. S., Watanabe, T., Maeda, H., Obata, A., & Kasuga, T. (2020). Preparation of an antibacterial amorphous thin film by radiofrequency magnetron sputtering using a 65ZnO–30P_2O_5–5Nb_2O_5 glass. *J Non-Cryst Solids*, *528*, 119724.
89. Moriishi, T., Ozasa, R., Ishimoto, T., Nakano, T., Hasegawa, T., Miyazaki, T., … Komori, H. . (2020). Osteocalcin is necessary for the alignment of apatite crystallites, but not glucose metabolism, testosterone synthesis, or muscle mass. *PLoS Genet*, *16*, e1008586.others

How to cite this article: Lee S, Nagata F, Kato K, Kasuga T, Nakano T. Development of orthophosphosilicate glass/poly (lactic acid) composite anisotropic scaffolds for simultaneous reconstruction of bone quality and quantity. *J Biomed Mater Res*. 2021;109:788–803. https://doi.org/10.1002/jbm.a.37067